Supplementary Material: A detailed PAH and soot model for complex fuels in CFD applications

Florian Eigentler[1*] and Peter Gerlinger[1]

[1*]Institute of Combustion Technology, German Aerospace Center (DLR), Pfaffenwaldring 38–40, Stuttgart, 70569, Baden-Württemberg, Germany.

*Corresponding author(s). E-mail(s): florian.eigentler@dlr.de;
Contributing authors: peter.gerlinger@dlr.de;

1 Laminar partially premixed ethylene flame

The influence of premixing on the soot tendency is investigated by McEnally and Pfefferle [1] for an atmospheric laminar sooting ethylene flame. The experiments are operated at three different equivalence ratios as described, together with the chosen boundary conditions, in Table 1. Corresponding simulations are performed on an axisymmetric grid (5° wedge) with approximately 25 000 volumes, and a predefined laminar inflow profile for the fuel feed.

The contour plots of temperature and soot volume fraction for the three equivalence ratios (Φ=3, 6 and 12) are shown in Fig. 1. Areas of high temperature become thinner with increasing Φ and soot volume fraction but extend

Table 1: Boundary conditions for the laminar partially premixed ethylene flame [1]. Given are inner r_i and outer r_o radius (mm), velocity v (mm/s), temperature T (K) and mass fractions Y_i (mass-%).

	fuel stream:						coflow stream:					
	r	v	T	$Y_{C_2H_4}$	Y_{O_2}	Y_{N_2}	r_i	r_o	v	T	Y_{O_2}	Y_{N_2}
$\Phi = 3$		349.7		13.12	3.73	81.58						
$\Phi = 6$	6	245.6	400	17.38	9.93	72.69	6.5	50	326.9	300	23	77
$\Phi = 12$		192.6		22.28	6.25	71.47						

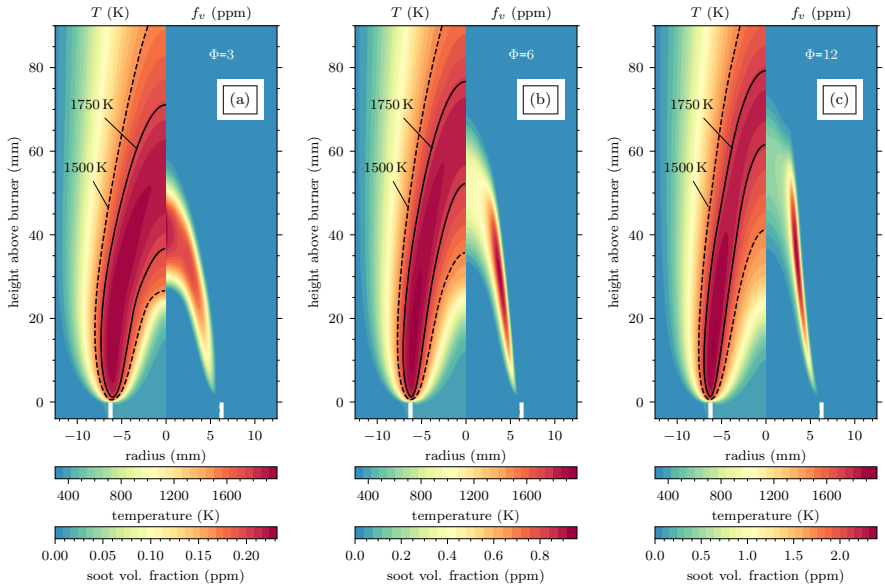

Fig. 1: Calculated temperature and soot volume fraction distributions for an atmospheric laminar partially premixed ethylene flame: (a) Φ=3, (b) Φ=6, and (c) Φ=12. Superimposed are iso-lines of two temperatures: 1500 K (dashed) and 1750 K (solid), on the left.

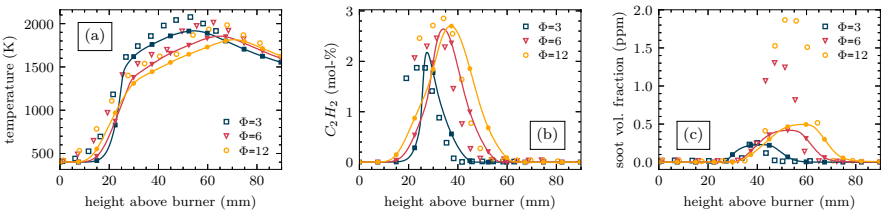

Fig. 2: Measured and calculated axial profiles in an atmospheric laminar partially premixed ethylene flame: (a) temperature, (b) C_2H_2 mole fraction, and (c) soot volume fraction. Open symbols: experimental data [1]; solid lines with filled symbols: calculated data.

further downstream despite lower inflow velocities (compare dashed and solid lines on the left side for 1500 K and 1750 K). In the leanest case most soot is formed in the area near the axis at a height of 40 mm. This shifts with increasing Φ towards the sideward flame front. The soot volume fraction distribution for Φ=12 already corresponds to the non-smoking diffusion flame investigated in Section 3.4.

Figure 2a shows that temperature trends with increasing amount of fuel are well reflected by the model. Experimental values are slightly underestimated, and the predicted increase in temperature near the burner inlet is located slightly further downstream than in the experiment. Measured mole fractions for C_2H_2 are compared with the simulation in Fig. 2b. Due to the lower temperatures near the burner inlet, the formation of C_2H_2 starts with an offset. However, except for this offset, the model reflects values and trends of this important soot growth species very well. Results of soot volume fraction on the burner axis are compared to the measurements in Fig. 2c. In all three simulations, the position of maximum soot volume fraction agrees perfectly with the experiment. For Φ=3 even the maximum value is in excellent agreement. However, for Φ=6 and 12 less soot is formed on the axis with a maximum deviation of factor 3.6. This may point to a missing path in soot formation, as identified in Section 3.5. Similar results have been obtained in other studies for this ethylene flame [2, 3]. Guo et al. [2] studied the influence of boundary conditions and found a significant impact on soot prediction. For this reason, and by the similar results compared to their works, the presented gas phase, polycyclic aromatic hydrocarbon (PAH) and soot model achieves very good agreement.

2 Sensitivity analysis of model components

With the introduction of the quasi-steady state for soot radicals in the definition of surface reactions in Eq. (9) (see Section 2.3 in the manuscript), an empirical constant (r_χ) has been introduced in the model. A value of 1.7×10^{-3} was found to be best suited throughout all experiments. To show the sensitivity of this parameter, shock tube experiments are recalculated with modified r_χ constants. In Fig. 3, only a single case of the studied shock tube experiments is shown. A detailed description of the experiments and boundary conditions can be found in Section 3.3 in the manuscript. As can be seen, clear improvements can neither be achieved with a halved ($r_\chi = 0.85 \times 10^{-3}$) nor with a doubled ($r_\chi = 3.4 \times 10^{-3}$) model constant. On the one hand, this justifies the chosen model constant ($r_\chi = 1.7 \times 10^{-3}$), and on the other hand, it shows the difficulty of defining a valid parameter for a large number of different fuels and operating conditions.

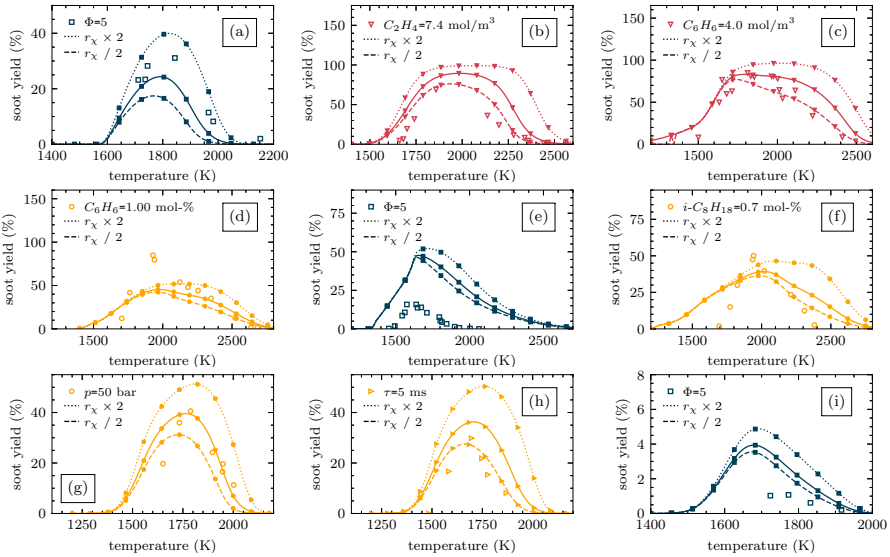

Fig. 3: Measured and calculated soot yields in the pyrolysis and oxidation of various hydrocarbon fuels: (a) methane, (b) ethylene, (c,d) benzene, (e) toluene, (f) toluene/iso-octane, (g,h) n-heptane, and (i) n-decane. Open symbols: experimental data [4–10]; solid lines with filled symbols: calculated data; dashed lines with filled symbols: calculated data with $\chi = 0.85 \times 10^{-3}$ (r_χ / 2); dotted lines with filled symbols: calculated data with $\chi = 3.4 \times 10^{-3}$ ($r_\chi \times 2$).

3 PAH model

Table 2: Summary of the gas phase interaction reactions with the first PAH section (PAH_1). Reaction rates are in Arrhenius form: $k = k_0 T^{\alpha} \exp(-T_a/T)$. Units are *mol*, *cm*, *s*, *K*.

PAH_1 formation			k_0	α	T_a
$A_1m + C_4H_2$	=	$\nu_{PAH_1}PAH_1 + C_2H$	2.00×10^{13}	0.00	11 000.00
$A_1m + C_2H_3$	=	$\nu_{PAH_1}PAH_1 + H_2$	7.90×10^{12}	0.00	3200.00
$A_1m + C_4H_4$	=	$\nu_{PAH_1}PAH_1 + C_2H_3$	3.20×10^{11}	0.00	680.36
$A_1 + C_2H$	=	$\nu_{PAH_1}PAH_1 + H$	5.00×10^{13}	0.00	0.00
$A_1m + C_2H$	=	$\nu_{PAH_1}PAH_1$	5.24×10^{14}	−0.50	300.00
$\nu_{PAH_1}PAH_1 + O$	=	$A_1m + HCCO$	2.10×10^{7}	2.00	950.00
$\nu_{PAH_1}PAH_1 + O$	=	$C_6H_5O + C_2H$	2.20×10^{13}	0.00	2260.00
$\nu_{PAH_1}PAH_1 + H$	=	$A_1m + C_2H_2$	2.00×10^{14}	0.00	4882.00
$\nu_{PAH_1}PAH_1 + OH$	=	$A_1m + CH_2CO$	2.18×10^{-4}	4.50	−500.00
$\nu_{PAH_1}PAH_1 + OH$	=	$A_1 + HCCO$	2.44×10^{3}	3.02	5574.00
$2C_4H_4$	=	$\nu_{PAH_1}PAH_1$	1.80×10^{20}	−1.90	20 230.00
$A_1 + C_2H_3$	=	$\nu_{PAH_1}PAH_1 + H$	7.90×10^{11}	0.00	3200.00
$A_1m + C_2H_3$	=	$\nu_{PAH_1}PAH_1$	1.06×10^{26}	−4.00	2650.00
$A_1m + C_2H_4$	=	$\nu_{PAH_1}PAH_1 + H$	2.51×10^{12}	0.00	3095.00
$A_1m + C_4H_4$	=	$\nu_{PAH_1}PAH_1 + C_2H$	4.00×10^{13}	0.00	10 000.00
$A_1m + C_4H_6$	=	$\nu_{PAH_1}PAH_1 + C_2H_3$	3.20×10^{11}	0.00	957.54
$C_7H_7 + CH_2$	=	$\nu_{PAH_1}PAH_1 + H$	2.40×10^{14}	0.00	0.00
$\nu_{PAH_1}PAH_1 + O$	=	$A_1m + CH_2HCO$	3.00×10^{8}	1.45	450.00
$\nu_{PAH_1}PAH_1 + O$	=	$A_1m + CH_3 + CO$	1.92×10^{7}	1.83	110.00
$\nu_{PAH_1}PAH_1 + O$	=	$C_2H_3 + C_6H_5O$	2.20×10^{13}	0.00	2265.00
$\nu_{PAH_1}PAH_1 + OH$	→	$C_6H_5O + C_2H_4$	1.30×10^{13}	0.00	5300.00
$\nu_{PAH_1}PAH_1 + OH$	=	$C_7H_7 + CH_2O$	1.40×10^{12}	0.00	0.00
$\nu_{PAH_1}PAH_1 + O_2$	=	$C_6H_5O + CH_2HCO$	1.88×10^{11}	0.00	3758.70
$C_5H_5 + H_2CCCH$	→	$\nu_{PAH_1}PAH_1$	1.00×10^{13}	0.00	4174.00
$C_7H_7 + CH_3$	→	$\nu_{PAH_1}PAH_1 + H_2$	1.06×10^{26}	−4.00	2650.00
$C_5H_5 + C_4H_4$	=	$\nu_{PAH_1}PAH_1 + H$	0.60×10^{12}	0.00	5030.00
$A_1m + H_2CCCH$	=	$\nu_{PAH_1}PAH_1$	3.86×10^{11}	0.00	6850.48
$C_4H_6 + A_1m$	=	$\nu_{PAH_1}PAH_1 + CH_3$	1.42×10^{13}	0.00	14 000.00
$A_1m + C_3H_4$	=	$\nu_{PAH_1}PAH_1 + H$	1.00×10^{16}	0.00	16 600.00
$\nu_{PAH_1}PAH_1 + O$	=	$C_7H_7 + HCCO$	2.00×10^{13}	0.00	2000.00
$C_7H_7 + C_2H_2$	=	$\nu_{PAH_1}PAH_1 + H$	0.60×10^{12}	0.00	5030.00
$\nu_{PAH_1}PAH_1 + H$	=	$A_1 + H_2CCCH$	2.00×10^{14}	0.00	24 500.00
$\nu_{PAH_1}PAH_1 + OH$	=	$C_7H_7 + CH_2CO$	1.00×10^{13}	0.00	5000.00
$C_5H_5 + H_2CCCCH$	=	$\nu_{PAH_1}PAH_1$	1.00×10^{13}	0.00	4174.00
$C_5H_5 + C_5H_6$	=	$\nu_{PAH_1}PAH_1 + CH_3$	9.63×10^{13}	1.63	29 972.00
$A_1m + A_1$	=	$\nu_{PAH_1}PAH_1 + H$	1.10×10^{23}	−2.92	7450.00
$2A_1m$	=	$\nu_{PAH_1}PAH_1$	2.00×10^{19}	−2.05	1450.00
$C_4H_6 + A_1m$	→	$\nu_{PAH_1}PAH_1 + H_2 + H$	5.00×10^{11}	0.00	1503.48
$A_1m + H_2CCCCH$	=	$\nu_{PAH_1}PAH_1$	3.18×10^{23}	−3.20	2130.00
$A_1m + C_4H_4$	=	$\nu_{PAH_1}PAH_1 + H$	3.30×10^{33}	−5.70	12 750.00
$C_7H_7 + H_2CCCH$	→	$\nu_{PAH_1}PAH_1 + 2\,H$	4.00×10^{11}	0.00	7000.00
$2C_5H_5$	→	$\nu_{PAH_1}PAH_1 + 2\,H$	3.00×10^{16}	0.00	23 625.00
$2C_5H_5$	→	$\nu_{PAH_1}PAH_1 + 2\,H$	4.53×10^{5}	1.83	18 041.00

Table 3: Summary of the gas phase interaction reactions with the first PAH radial section (PAH_1^*). Reaction rates are in Arrhenius form: $k = k_0 T^{\alpha} \exp(-T_a/T)$. Units are *mol*, *cm*, *s*, *K*.

PAH_1^* formation			k_0	α	T_a
$H_2CCCCH + C_4H_2$	$\rightarrow$	$\nu_{PAH_1^*} PAH_1^*$	9.60×10^{70}	-17.77	15 660.00
$C_5H_5 + H_2CCCH$	=	$\nu_{PAH_1^*} PAH_1^* + H$	3.00×10^{35}	-7.18	4234.00
$C_5H_5 + H_2CCCH$	=	$\nu_{PAH_1^*} PAH_1^* + H$	1.50×10^{35}	-7.18	4234.00
$A_1 + C_2H$	$\rightarrow$	$\nu_{PAH_1^*} PAH_1^*$	7.00×10^{38}	-8.02	8200.00
$A_1m + C_2H_2$	$\rightarrow$	$\nu_{PAH_1^*} PAH_1^*$	4.00×10^{13}	0.00	5878.00
$A_1m + C_2H_3$	=	$\nu_{PAH_1^*} PAH_1^* + H$	9.40	4.14	11 617.00
$C_5H_5 + C_4H_2$	=	$\nu_{PAH_1^*} PAH_1^*$	1.20×10^{12}	0.00	5030.00
$\nu_{PAH_1^*} PAH_1^*$	$\rightarrow$	$C_2H_2 + C_4H_2 + H_2CCCH$	1.00×10^{14}	0.00	37 500.00
$2C_5H_5$	=	$\nu_{PAH_1^*} PAH_1^* + CH_3$	2.50×10^{12}	0.00	4811.00
$2A_1m$	=	$\nu_{PAH_1^*} PAH_1^* + H$	2.30×10^{-1}	4.62	14 500.00
$A_1m + H_2CCCCH$	=	$\nu_{PAH_1^*} PAH_1^* + H$	2.00×10^{-10}	7.10	786.19

Table 4: Summary of the PAH model. Reaction rates are in Arrhenius form: $k = k_0 T^{\alpha} \exp(-T_a/T)$. Units are *mol*, *cm*, *s*, *K*.

Hydrogen abstraction ($i \in [1,3]$)			k_0	α	T_a
$PAH_i + OH$	=	$PAH_i^* + H_2O$	2.10×10^{13}	0.00	2300.00
$PAH_i + H$	=	$PAH_i^* + H_2$	2.50×10^{14}	0.00	8000.00
$PAH_i^* + H$	=	PAH_i	1.00×10^{14}	0.00	0.00
$PAH_i + O$	=	$PAH_i^* + OH$	2.00×10^{13}	0.00	7400.00
Carbon addition ($i \in [1,3]$)			k_0	α	T_a
$PAH_i^* + C_2H_2$	$\rightarrow$	$\nu_{PAH_i} PAH_i + \nu PAH_{i+1} + \nu H$	1.60×10^{16}	-1.33	3300.00
$PAH_i^* + C_4H_2$	$\rightarrow$	$\nu_{PAH_i} PAH_i + \nu PAH_{i+1}$	1.60×10^{16}	-1.33	2700.00
Collision ($i, j \in [1,3]$, $k = max(i,j)$)			k_0	α	T_a
$PAH_i^* + PAH_j$ $\rightarrow \nu_{PAH_k} PAH_k + \nu_{PAH_{k+1}} PAH_{k+1} + \nu_{H_2} H_2$ $PAH_i^* + PAH_j^*$ $\rightarrow \nu_{PAH_k} PAH_k + \nu_{PAH_{k+1}} PAH_{k+1} + \nu_{H_2} H_2 + \nu_H H$			Sec. 2.2 Eq. (3), $\gamma_{i,j} = 1.0$		
Oxidation ($i \in [1,3]$)			k_0	α	T_a
$PAH_i^* + O_2$ $\rightarrow \nu_{PAH_{i-1}^*} PAH_{i-1}^* + \nu_{PAH_i^*} PAH_i^* + \nu_{H_2} H_2$ $+ \nu_{CO} CO + \nu HCO$			1.00×10^{11}	0.00	3700.00
$PAH_i^* + HO_2$ $\rightarrow \nu_{PAH_{i-1}^*} PAH_{i-1}^* + \nu_{PAH_i^*} PAH_i^* + \nu_{H_2} H_2$ $+ \nu_{CO} CO + \nu OH$			1.00×10^{13}	0.00	0.00
$PAH_i + OH$ $\rightarrow \nu_{PAH_{i-1}^*} PAH_{i-1}^* + \nu_{PAH_i^*} PAH_i^* + \nu_{H_2} H_2$ $+ \nu CH_2CO$			1.30×10^{13}	0.00	5300.00
$PAH_i + O$ $\rightarrow \nu_{PAH_{i-1}^*} PAH_{i-1}^* + \nu_{PAH_i^*} PAH_i^* + \nu_{H_2} H_2$ $+ \nu HCCO$			2.00×10^{13}	0.00	21 000.00
$PAH_i^* + O$ $\rightarrow \nu_{PAH_{i-1}^*} PAH_{i-1}^* + \nu_{PAH_i^*} PAH_i^* + \nu_{H_2} H_2$ $+ \nu_{CO} CO$			1.00×10^{14}	0.00	0.00

4 Soot model

Table 5: Summary of the soot model. Reaction rates are in Arrhenius form: $k = k_0 T^{\alpha} \exp(-T_a/T)$. Units are *mol*, *cm*, *s*, *K*.

Condensation ($i \in [1, 30]$)	k_0	α	T_a
$SOOT_i + C_2H_2 \rightarrow \nu_{SOOT_i} SOOT_i + \nu_{SOOT_{i+1}} SOOT_{i+1} + \nu_{H_2} H_2$	8.00×10^7	1.56	1912.00
$SOOT_i + C_4H_2 \rightarrow \nu_{SOOT_i} SOOT_i + \nu_{SOOT_{i+1}} SOOT_{i+1} + \nu_{H_2} H_2$	4.00×10^{13}	0.00	6038.00
$SOOT_i + C_6H_2 \rightarrow \nu_{SOOT_i} SOOT_i + \nu_{SOOT_{i+1}} SOOT_{i+1} + \nu_{H_2} H_2$	4.00×10^{13}	0.00	4025.00
$SOOT_i + C_8H_2 \rightarrow \nu_{SOOT_i} SOOT_i + \nu_{SOOT_{i+1}} SOOT_{i+1} + \nu_{H_2} H_2$	4.00×10^{13}	0.00	1509.00
$SOOT_i + C_{10}H_2 \rightarrow \nu_{SOOT_i} SOOT_i + \nu_{SOOT_{i+1}} SOOT_{i+1} + \nu_{H_2} H_2$	4.00×10^{13}	0.00	0.00
$SOOT_i + C_{12}H_2 \rightarrow \nu_{SOOT_i} SOOT_i + \nu_{SOOT_{i+1}} SOOT_{i+1} + \nu_{H_2} H_2$	4.00×10^{13}	0.00	0.00
PAH collision, ($i \in [1, 30]$, $j \in [1, 3]$)	k_0	α	T_a
$SOOT_i + PAH_j \rightarrow \nu_{SOOT_i} SOOT_i + \nu_{SOOT_{i+1}} SOOT_{i+1} + \nu_{H_2} H_2$	Sec. 2.2 Eq. (3), $\gamma_{i,j} = 0.3$		
$SOOT_i + PAH_j^* \rightarrow \nu_{SOOT_i} SOOT_i + \nu_{SOOT_{i+1}} SOOT_{i+1} + \nu_H H$			
Oxidation ($i \in [1, 30]$)	k_0	α	T_a
$SOOT_i + O_2 \rightarrow \nu_{SOOT_{i-1}} SOOT_{i-1} + \nu_{SOOT_i} SOOT_i + \nu_{H_2} H_2 + \nu_{CO} CO$	2.20×10^{12}	0.00	3774.36
$SOOT_i + OH \rightarrow \nu_{SOOT_{i-1}} SOOT_{i-1} + \nu_{SOOT_i} SOOT_i + \nu_{H_2} H_2 + \nu_{CO} CO$	8.82×10^6	0.50	0.00
Agglomeration ($i, j \in [1, 30]$, $k = max(i, j)$)	k_0	α	T_a
$SOOT_i + SOOT_j \rightarrow \nu_{SOOT_k} SOOT_k + \nu_{SOOT_{k+1}} SOOT_{k+1} + \nu_{H_2} H_2$	Sec. 2.2 Eq. (3), $\gamma_{i,j} = 1.0$		

References

[1] McEnally, C.S., Pfefferle, L.D.: Experimental study of nonfuel hydrocarbons and soot in coflowing partially premixed ethylene/air flames. Combust. Flame **121**(4), 575–592 (2000). https://doi.org/10.1016/s0010-2180(99)00174-1

[2] Guo, H., Liu, F., Smallwood, G.J., Gülder, Ö.L.: The flame preheating effect on numerical modelling of soot formation in a two-dimensional laminar ethylene–air diffusion flame. Combust. Theory Model. **6**(2), 173–187 (2002). https://doi.org/10.1088/1364-7830/6/2/301

[3] Chernov, V., Zhang, Q., Thomson, M.J., Dworkin, S.B.: Numerical investigation of soot formation mechanisms in partially-premixed ethylene–air

co-flow flames. Combust. Flame **159**(9), 2789–2798 (2012). https://doi.org/10.1016/j.combustflame.2012.02.023

[4] Kellerer, H., Müller, A., Bauer, H.-J., Wittig, S.: Soot formation in a shock tube under elevated pressure conditions. Combust. Sci. Technol. **113**(1), 67–80 (1996). https://doi.org/10.1080/00102209608935488

[5] Vlasov, P.A., Warnatz, J.: Detailed kinetic modeling of soot formation in hydrocarbon pyrolysis behind shock waves. Proc. Combust. Inst. **29**(2), 2335–2341 (2002). https://doi.org/10.1016/s1540-7489(02)80284-x

[6] Agafonov, G.L., Vlasov, P.A., Smirnov, V.N.: Soot formation in the pyrolysis of benzene, methylbenzene, and ethylbenzene in shock waves. Kinet. Catal. **52**(3), 358–370 (2011). https://doi.org/10.1134/s0023158411030013

[7] Agafonov, G.L., Naydenova, I., Vlasov, P.A., Warnatz, J.: Detailed kinetic modeling of soot formation in shock tube pyrolysis and oxidation of toluene and n-heptane. Proc. Combust. Inst. **31**(1), 575–583 (2007). https://doi.org/10.1016/j.proci.2006.07.191

[8] Alexiou, A., Williams, A.: Soot formation in shock-tube pyrolysis of toluene-n-heptane and toluene-iso-octane mixtures. Fuel **74**(2), 153–158 (1995). https://doi.org/10.1016/0016-2361(95)92648-p

[9] Hong, Z., Davidson, D., Hanson, R.: Shock tube studies of soot formation in heptane and heptane/DME mixtures. In: 45th AIAA Aerospace Sciences Meeting and Exhibit, paper AIAA 2007-774, American Institute of Aeronautics and Astronautics (2007). https://doi.org/10.2514/6.2007-774

[10] Bockhorn, H.: Soot Formation In Combustion - Mechanisms And Models. Springer, Berlin Heidelberg (2013)